Macromolecules
ARTICLE

Macromolecules **2010**, *43*, 1539–1542 **1539**
DOI: 10.1021/ma902324f

Chain Deformation in Entangled Polymer Melts at Re-entrant Corners

N. Clarke,* E. De Luca, G. Buxton, and L. R. Hutchings

Department of Chemistry, Durham University, Durham DH1 3LE, U.K.

T. Gough

School of Engineering, Design and Technology, University of Bradford, Bradford BD7 1DP, U.K.

I. Grillo

Institut Laue Langevin, 6 rue Jules Horowitz, BP 156 38042 Grenoble Cedex 9, France

R. S. Graham

School of Mathematical Sciences, University of Nottingham, Nottingham NG7 2RD, U.K.

K. Jagannathan and D. H. Klein

Department of Physics and Astronomy, University of Leeds, Leeds LS2 9JT, U.K.

T. C. B. McLeish

Departments of Physics and Chemistry, Durham University, Durham DH1 3LE, U.K.

Received October 19, 2009; Revised Manuscript Received December 23, 2009

ABSTRACT: Using SANS to map the deformation of individual polymer chains in the vicinity of re-entrant corners in a contraction−expansion flow, we show that stress singularities at such corners, predicted by formulations of fluid dynamics that lack a molecular basis, do not cause extreme deformation of the chains. Multiscale modeling based on a nonlinear tube theory incorporating appropriate relaxation processes quantitatively reproduces the observed scattering, thus providing further evidence for the universality of the tube model for polymer flow.

1. Introduction

Formulations of both Newtonian and non-Newtonian fluid dynamics predict stress singularities at re-entrant corners[1−6] (see Figure 1) and have therefore fascinated both experimental and theoretical rheologists. From a practical viewpoint, the existence of such singularities has hampered the development of quantitative tools for predicting fluid flow in geometries that include re-entrant corners, ubiquitous in polymer processing. The subclass of flows that contain a contraction, and subsequent expansion, are particularly challenging theoretically, not just because of the stress singularity but also because a successful model must correctly describe the viscous and elastic stresses that arise in both elongation and shear over the wide range of velocity gradients present. Furthermore, the slow relaxation of stresses and large-scale chain conformations in polymer melts means that memory effects are important: how a chain responds to a shear or elongational flow at any given position depends not only on the instantaneous velocity gradients but also on the flow profile along the path it has taken to arrive at that position.

The way in which a polymeric fluid responds at a re-entrant corner has implications for not just macroscopic phenomena such as helical defects and melt fracture[7] but also for microscopic phenomena such as the orientation and stretch of individual polymer chains. Chain deformation induced during processing is often retained in the solid state upon freezing or vitrification. Anisotropy at larger length scales controls, for example, nonlinear deformation properties of the solid phase for both semicrystalline and amorphous polymers.[8] Such anisotropy is implicit in tube models, which recognize that polymeric stress arising only from the local bond orientation distribution does not determine the chain conformations completely.

For Newtonian fluids, in which the viscosity is independent of the flow rate, the stress diverges as $r^{-0.4555}$, where r is the radial distance from the corner.[2] For shear thickening or shear thinning power-law fluids, in which the viscosity increases with shear rate, $\dot{\gamma}$, as $\dot{\gamma}^{0.5}$ or decreases as $\dot{\gamma}^{-0.5}$, the stress diverges as $r^{-0.54}$ and $r^{-0.31}$, respectively.[4] For non-Newtonian fluids characterized by at least one finite stress relaxation time, the picture is more complex. For example, for the upper convected Maxwell model, the simplest mathematical description of a viscoelastic fluid, it has been shown analytically[3,5] that the stress diverges as $r^{-2/3}$, while computational studies[1,6] suggest that the divergence is between $r^{-0.9}$ and r^{-1}. This discrepancy remains unresolved and highlights the challenges associated with understanding the flow of non-Newtonian fluids around sharp corners. Adopting an alternative approach to continuum modeling, Koplic and Banavar[9] used molecular dynamics to model the flow of low molecular weight unentangled polymer melts around a sharp corner. While such modeling is valuable in aiding our understanding of what

*Corresponding author. E-mail: nigel.clarke@durham.ac.uk.

Published on Web 01/07/2010

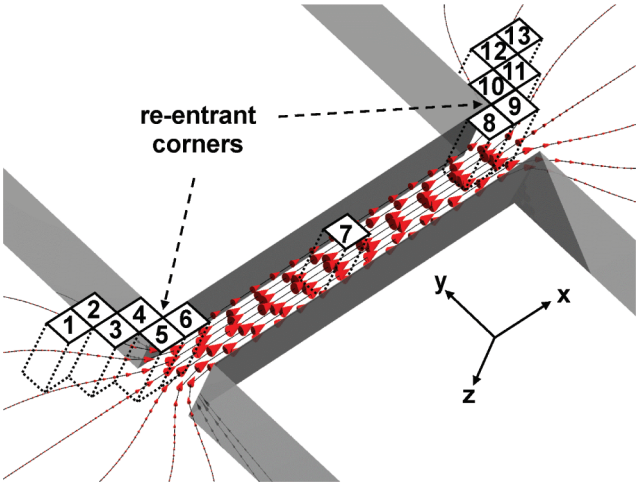

Figure 1. Schematic of the geometry of the flow cell illustrating the regions of the flow at which the scattering was measured. The neutron beam is incident in the z direction.

might be happening at the molecular level, the length and time scales involved in typical polymer processing, and the much more demanding computational requirements for entangled melts, are such that molecular-based continuum models will continue to be the method of choice.

Experimentally, the predicted singularities must be moderated by molecular-scale physics. However, the question of how a fluid avoids the divergence remains unresolved since most experimental probes of the flow response only reflect behavior at length scales much larger than that of the macromolecules. Such probes include particle image velocimetry,[10] birefringence,[11] and pressure drop measurements.[12] In contrast, small-angle neutron scattering (SANS) is ideally suited to measuring the stretching and orientation of individual chains. In this paper, we provide the first experimental confirmation that a molecularly based description of the flow behavior is able to correctly describe the chain deformation both within the vicinity of, and away from, the re-entrant corner. By comparing the neutron flow-mapping experiments with multiscale calculations based on an advanced formulation of the tube model for entangled polymers, we elucidate the importance of the rapid process of chain retraction within tubes. We find that the singularity is strongly suppressed, to the extent that it is at least integrable, and we are able to correctly predict the chain deformation within the vicinity of the re-entrant corner.

2. Experimental Section

Materials. Deuterated polystyrene, dPS (M_w = 264 000 g mol^{-1}, Pd = 1.12), and hydrogenous polystyrene, PS (M_w = 271 000 g mol^{-1}, Pd = 1.06), were synthesized by anionic polymerization using standard high-vacuum techniques. Benzene was used as the solvent and *sec*-butyllithium as the initiator. To obtain a 95/5 w/w blend of dPS/PS and to ensure blending at a molecular level, the two polymers were dissolved in THF at 5% w/v and stirred in solution for an hour. The blend was recovered by precipitation by adding the polymer solution to ~10 times the volume of a nonsolvent, methanol. The resulting precipitate was collected by filtration and dried to constant mass in vacuo.

Flow Cell. The recirculating flow cell[13] enables a steady-state flow in contraction−expansion geometry to be achieved and has been previously used to measure the single chain structure factor in monodisperse[8,14] and bidisperse[15] polymer melts and linear/branched polymer mixtures[16] and concentration fluctuations in polymer blends[17] under flow. All previous measurements have been confined to the centerline of the flow. The width of the cell prior to and after the contraction is 10 mm while within the contraction it is 2.5 mm, so that we have a 4:1 contraction−expansion. The length of the contraction is 20 mm, and the thickness of the cell is 10 mm throughout, in order that the flow field in the vicinity of the contraction remains approximately 2-dimensional. For the experiments described herein, the volumetric flow rates through the cell are 0.22 and 0.38 cm^3/s, which correspond to wall shear rates within the contraction of $\dot{\gamma}_{wall}$ = 21 s^{-1} and $\dot{\gamma}_{wall}$ = 36 s^{-1} and maximum extensional rates along the centerline of $\dot{\varepsilon}_{max}^{centerline}$ = 3.9 s^{-1} and $\dot{\varepsilon}_{max}^{centerline}$ = 6.7 s^{-1}, respectively.

Small-Angle Neutron Scattering. SANS was performed on the D22 diffractometer at the Institute Laue-Langevin (Grenoble, France). We illuminated sample areas of 1 mm by 1 mm at various positions as illustrated in Figure 1 with a fixed neutron wavelength of 10 Å. The sample-to-detector distance and the collimation distance were both set at 5.6 m to optimize the flux and the resolution. With a detector offset of 400 mm, the q range accessed was $0.007 < q/\text{Å}^{-1} < 0.13$. Water was used to measure the detector efficiency and for data normalization. The raw data were corrected for empty cell background and absorption and normalized to the absolute cross section prior to analysis.

Rheology. Relaxation times for the modeling were determined using frequency sweep measurements on the blend, performed using a TA AR2000 rheometer with plate−plate geometry (radius of 25 mm and gap 1.1 mm) at a temperature of 473 K.

3. Theory

The nonlinear tube model, GLaMM,[18] has been used to predict the SANS patterns from entangled polymers under strong flow.[8,14,19] In the model, the relaxation mechanisms of reptation, contour length fluctuations, retraction, and constraint release are formulated into a stochastic microscopic evolution equation for the dynamics of the space curve describing the tube contour. From this equation a deterministic partial differential equation for the tube tangent vector correlation function is derived, allowing the average tube configuration, stress tensor, and the single chain structure factor to be computed for any nonlinear deformation.[8,18] Of particular importance is that the parameters of the GLaMM theory are found by fitting a linear tube theory[20] to the independent linear oscillatory shear measurements on the melt. Using a value for the molecular weight between entanglements of M_e = 16 400, such that our dPS melt has 16 entanglements and a Rouse time of an entanglement segment, $\tau_e = 12.7 \times 10^{-6}$ s (consistent with previous measurements[8,14]), gives a reptation time of τ_{rep} = 0.067 s and a Rouse time of τ_R = 0.0034 s at 220 °C . Hence the dimensionless numbers corresponding to the higher flow rate are $\dot{\gamma}_{wall}\tau_e = 4.6 \times 10^{-4}$, $\dot{\gamma}_{wall}\tau_R$ = 0.12, $\dot{\gamma}_{wall}\tau_{rep}$ = 2.4, $\dot{\varepsilon}_{max}^{centerline}\tau_e = 8.5 \times 10^{-5}$, $\dot{\varepsilon}_{max}^{centerline}\tau_R$ = 0.023, and $\dot{\varepsilon}_{max}^{centerline}\tau_{rep}$ = 0.45. Consequently, the flow can be considered weakly nonlinear, and since Rouse Weissenberg numbers are less than unity, the flow is nonstretching over most of the domain. To characterize the scattering, values for the tube diameter, a = 78 Å, and the scattering at zero wavevector, I_0 = 33.7 cm^{-1}, were obtained from the literature[8] and checked against our quiescent scattering data using the Debye model.

Although a detailed treatment of the GLaMM theory is required to compute scattering patterns from a given flow field, it is unfeasible, with present computing power, to also use this model for a finite element flow computation. We have found however that an accurate calculation of the flow field requires only a simpler constitutive equation capable of computing the stress tensor. To compute the steady-state velocity field, we used a simplified version of the GLaMM theory, known as the Rolie-Poly constitutive equation,[18,21] in a multimode version, with parameters fitted to our rheological data and the predictions of the GLaMM model in shear. Our in-house Lagrangian viscoelastic code, flowSolve,[22] was used to provide the deformation history for all streamlines passing through all regions sampled by

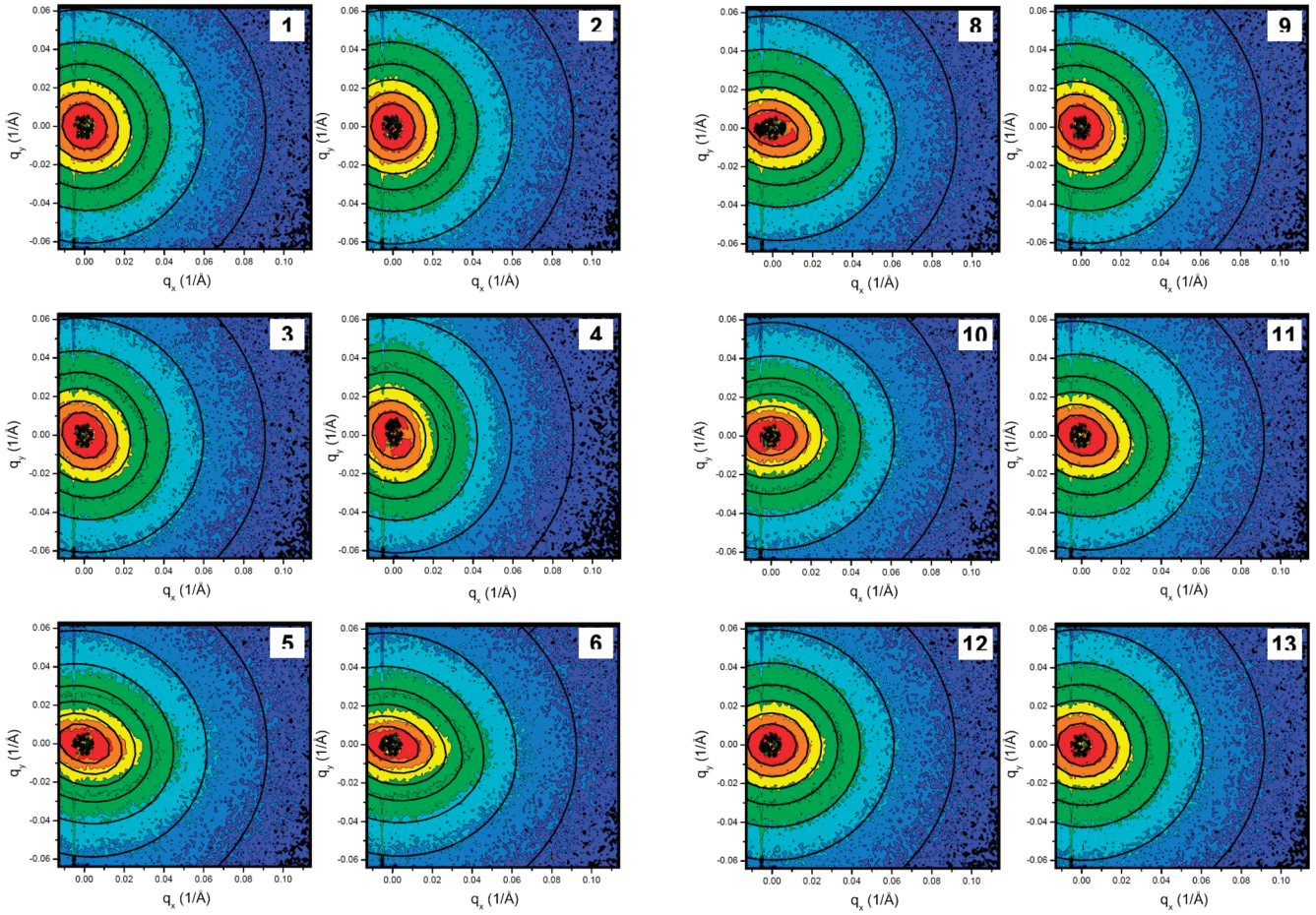

Figure 2. GLaMM theory predictions overlaid on the measuring scattering patterns for (1−6) regions upstream from the contraction and (8−13) regions downstream from the contraction. The numbers on each figure correspond to the labeling in Figure 1. The data for position 7, along the centerline, is not shown since it corresponds to data previously presented in refs 8 and 14.

the neutron beam. We then assume that molecules are advected along with fluid elements, that the chains move along the stream lines, and that there is no diffusion of chains between streamlines with significantly different velocity gradients. This is reasonable since over the time scale of the terminal relaxation time, the chain diffuses a distance comparable to its radius of gyration, which is very small compared to the macroscopic dimensions of the flow cell. Thus, we compute the velocity gradient tensor along a set of streamlines that lead into the neutron sampling region and use these velocity gradient histories as input to the GLaMM model to predict the SANS patterns. For the moderate nonlinear flows that arise in our experiments, we assume[8,23] that the separation between two monomers, s and s', on the same chain, have a Gaussian distribution with the mean-squared separation provided by the GLaMM model. The variation of the scattering pattern across the length and width of each square region sampled by the neutron beam was accounted for by splitting each region into a 5 by 5 grid and computing the scattering from the streamline history of each individual point and finally summing. Generally the variation across each individual neutron scattering region was small, and good convergence was found using 25 grid points, indicating relatively uniform scattering across each neutron sampling region.

4. Results and Discussion

In Figure 2, we show the scattering from various positions within the flow cell for the highest volumetric flow rate. As can be seen, the scattering patterns in the q_x, q_y plane are elliptically deformed because of the deformation history of the polymer chains, but in this case the flow direction also influences the scattering patterns. In particular, the chains are no longer simply elongated or contracted in the flow direction but exhibit both elongation and rotation in the highly sheared regions of the cell, as can be seen from the changing orientation of the principal axis of the single chain scattering patterns.

The data can be fit reasonably well, at least for $qR_g \leq 1$, using the empirical relation $S_0/S(q) = 1 + (R_{g1}{}^2q_1{}^2 + R_{g2}{}^2q_2{}^2)/3$. Hence, we can determine the direction of maximum deformation and the two radii of gyration perpendicular and parallel to the axis of maximum deformation. Of particular interest is the variation of the radii of gyration from the quiescent value, which gives a simple measure of polymer chain deformation due to the flow field. Hence, we normalize R_{g1} and R_{g2} to the radius of gyration of the quiescent sample ($R_{g0} = 14.5$ nm) and obtain a measure of relative deformation along the major and minor axis. The results of these calculations are summarized in Figure 3. We find that the extent of chain anisotropy varies from 6% to nearly 40% at different positions within the cell. The greatest anisotropy occurs, as would be expected, at the re-entrant corner. At the higher flow rate, $\dot{\varepsilon}_{max}^{centerline}\tau_{rep} = 0.45$, at most positions the chain deformation is increased by a further ∼10−15% compared to the value at $\dot{\varepsilon}_{max}^{centerline}\tau_{rep} = 0.26$. A notable exception occurs at position 10, where the chains are apparently stretched by a further 22%. In the direction perpendicular to the main axis of stretch, we find that the variation in the radius of gyration is much less; for the lower flow rate, the range of decrease is from ∼7% to 15%, whereas at the higher flow rate the decrease in the radius of gyration with respect to a relaxed chain is actually slightly less, from 4% to 14%.

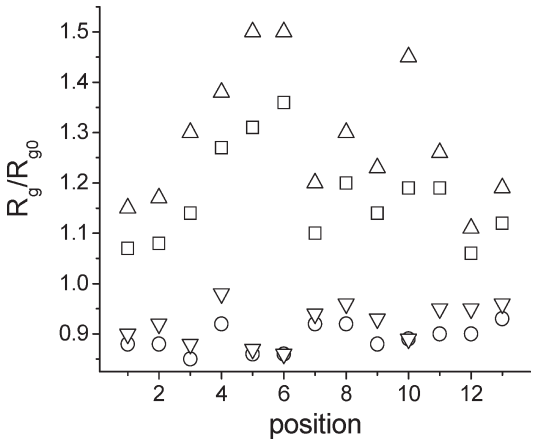

Figure 3. Radius of gyration along the major (flow rates: □, 0.22 $cm^3 s^{-1}$; △, 0.38 $cm^3 s^{-1}$) and minor axis (flow rates: ▽, 0.22 $cm^3 s^{-1}$; ○, 0.38 $cm^3 s^{-1}$) using the empirical relation $S_0/S(q) = 1 + (R_{g1}^2 q_1^2 + R_{g2}^2 q_2^2)/3$.

Although the above analysis provides an estimate of the degree of stretching of the chains, the fitting function is unable to describe the full subtlety of the length-scale dependence of the chain stretching, particularly for $qR_g > 1$. For this we turn to the GLaMM model. A comparison of the measured scattering patterns with the predictions of this theory is shown in Figure 2. Generally, the variation of degree of anisotropy and angle of tilt with length scale (i.e., q vector) is quantitatively predicted by the model for all regions of neutron sampling. We emphasize that the model predicts not just the overall extent of deformation, as measured by the scattering in the limit of $q \rightarrow 0$, but also the q dependence for length scales less than the radius of gyration. We also incorporate scattering for subtube length scales by assuming that monomer fluctuations about the mean path defined by the tube are isotropic and not correlated to tube deformation.[8,19] Furthermore, there are no adjustable parameters required to fit the data; all parameters are determined from independent linear rheology and quiescent scattering measurements. At regions of higher strain, the model slightly under predicts the degree of rotation and anisotropy, which is in contrast to an overprediction of the anisotropy in extensional flow along the centerline.[8] Notably, the underprediction of the anisotropy is most significant at position 10, which is the region in which the difference in radius of gyration along the streamline is greatest between the two flow rates. This result suggests that for the highest deformation gradients the model is slightly overestimating the extent of stretch relaxation.

5. Conclusions

This paper provides the first experimental confirmation of the GLaMM theory's ability to predict chain deformation and the subsequent chain structure factor, in a shear dominated flow that includes a re-entrant corner. Our results show how a polymer melt is able to effectively relax stress in a strong shear at a re-entrant corner by making use of molecular processes such as stretch relaxation and convective constraint release. The effectiveness of these processes, which both rely on the much faster curvilinear Rouse stretch relaxation, suggests a possible explanation for the phenomenon of melt fracture. We speculate this may arise in flows that are too strong, such that, $\dot{\gamma}\tau_R, \dot{\varepsilon}\tau_R > 1$, for these various relaxation mechanisms to be effective in moderating the stress divergence. In summary, we now possess the tools to predict the configuration of whole chains in a complex flow geometry over a range of length scales. This is an essential component in any molecular design methodology for future polymer processes.

References and Notes

(1) Coates, P. J.; Armstrong, R. C.; Brown, R. A. *J. Non-Newtonian Fluid Mech.* **1992**, *42*, 141–188.
(2) Dean, W. R.; Montagnon, P. E. *Proc. Cambridge Philos. Soc.* **1949**, *45*, 389–394.
(3) Evans, J. D. *Proc. R. Soc. London, Ser. A* **2005**, *461*, 117–142.
(4) Henriksen, P.; Hassager, O. *J. Rheol.* **1989**, *33*, 865–879.
(5) Hinch, E. J. *J. Non-Newtonian Fluid Mech.* **1993**, *50*, 161–171.
(6) Lipscomb, G. G.; Keunings, R.; Denn, M. M. *J. Non-Newtonian Fluid Mech.* **1987**, *24*, 85–96.
(7) Tordella, J. P. *J. Appl. Phys.* **1956**, *27*, 454–458.
(8) Graham, R. S.; Bent, J.; Hutchings, L. R.; Richards, R. W.; Groves, D. J.; Embery, J.; Nicholson, T. M.; McLeish, T. C. B.; Likhtman, A. E.; Harlen, O. G.; Read, D. J.; Gough, T.; Spares, R.; Coates, P. D.; Grillo, I. *Macromolecules* **2006**, *39*, 2700–2709.
(9) Koplik, J.; Banavar, J. R. *Phys. Rev. Lett.* **1997**, *78*, 2116–2119.
(10) Ballenge, T. F.; White, J. L. *J. Appl. Polym. Sci.* **1971**, *15*, 1949–1962.
(11) Bagley, E. B.; Birks, A. M. *J. Appl. Phys.* **1960**, *31*, 556–561.
(12) Rothstein, J. P.; McKinley, G. H. *J. Non-Newtonian Fluid Mech.* **1999**, *86*, 61–88.
(13) Bent, J. F.; Richards, R. W.; Gough, T. D. *Rev. Sci. Instrum.* **2003**, *74*, 4052–4057.
(14) Bent, J.; Hutchings, L. R.; Richards, R. W.; Gough, T.; Spares, R.; Coates, P. D.; Grillo, I.; Harlen, O. G.; Read, D. J.; Graham, R. S.; Likhtman, A. E.; Groves, D. J.; Nicholson, T. M.; McLeish, T. C. B. *Science* **2003**, *301*, 1691–1695.
(15) Graham, R. S.; Bent, J.; Clarke, N.; Hutchings, L. R.; Richards, R. W.; Gough, T.; Hoyle, D. M.; Harlen, O. G.; Grillo, I.; Auhl, D.; McLeish, T. C. B. *Soft Matter* **2009**, *5*, 2383–2389.
(16) McLeish, T. C. B.; Clarke, N.; de Luca, E.; Hutchings, L. R.; Graham, R. S.; Gough, T.; Grillo, I.; Fernyhough, C. M.; Chambon, P. *Soft Matter* **2009**, *5*, 4426–4432.
(17) Clarke, N.; De Luca, E.; Bent, J.; Buxton, G.; Gough, T.; Grillo, I.; Hutchings, L. R. *Macromolecules* **2006**, *39*, 7607–7616.
(18) Graham, R. S.; Likhtman, A. E.; McLeish, T. C. B. *J. Rheol.* **2003**, *47*, 1171–1200.
(19) Blanchard, A.; Graham, R. S.; Heinrich, M.; Pyckhout-Hintzen, W.; Richter, D.; Likhtman, A. E.; McLeish, T. C. B.; Read, D. J.; Straube, E.; Kohlbrecher, J. *Phys. Rev. Lett.* **2005**, *95*, 1660011–1660014.
(20) Likhtman, A. E.; McLeish, T. C. B. *Macromolecules* **2002**, *35*, 6332–6343.
(21) Likhtman, A. E.; Graham, R. S. *J. Non-Newtonian Fluid Mech.* **2003**, *114*, 1–12.
(22) Bishko, G. B.; Harlen, O. G.; McLeish, T. C. B.; Nicholson, T. M. *J. Non-Newtonian Fluid Mech.* **1999**, *82*, 255–273.
(23) Milner, S. T.; McLeish, T. C. B.; Likhtman, A. E. *J. Rheol.* **2001**, *45*, 539–563.